Structural elucidation of ubiquitin via gas-phase ion/ion cross-linking reactions using sodium-cationized reagents coupled with infrared multiphoton dissociation

Woo-Young Kang, Arup Mondal, Julia R. Bonney, Alberto Perez, Boone M. Prentice*

Department of Chemistry, University of Florida

*Address correspondence to:
Dr. Boone M. Prentice
214 Leigh Hall
PO Box 117200
Department of Chemistry
University of Florida
Gainesville, FL 32611, USA
Phone: (352) 392-0556
Fax: (352) 392-4651
Email: booneprentice@chem.ufl.edu

Keywords: ion/ion reactions, cross-linking mass spectrometry, sodiated cross-linker anions, internal fragment ions

ABSTRACT

Accurate structural determination of proteins is critical to understanding their biological functions and the impact of structural disruption on disease progression. Gas-phase cross-linking mass spectrometry (XL-MS) via ion/ion reactions between multiply charged protein cations and singly charged cross-linker anions has previously been developed to obtain low-resolution structural information of proteins. This method significantly shortens experimental time relative to conventional solution-phase XL-MS, but has several technical limitations, including (1) the singly deprotonated, N-hydroxysulfosuccinimide (sulfo-NHS)-based cross-linker anions are restricted to attachment at neutral amine groups of basic amino acid residues and (2) analyzing terminal cross-linked fragment ions is insufficient to unambiguously localize sites of linker attachment. Herein, we demonstrate enhanced structural information for alcohol-denatured A-state ubiquitin obtained from an alternative gas-phase XL-MS approach. Briefly, singly sodiated ethylene glycol bis(sulfosuccinimidyl succinate) (sulfo-EGS) cross-linker anions enable covalent cross-linking at both ammonium and amine groups. Additionally, covalently modified internal fragment ions, along with terminal b-/y-type counterparts, improve the determination of linker attachment sites. Molecular dynamics simulations validate experimentally obtained gas-phase conformations of denatured ubiquitin obtained herein. This method has identified four cross-linking sites across 8+ ubiquitin, including two new sites in the N-terminal region of the protein that were originally inaccessible in prior gas-phase XL approaches. The two N-terminal cross-linking sites suggest that the N-terminal half of ubiquitin is more compact in gas-phase conformations. By comparison, the two C-terminal linker sites indicate the signature transformation of this region of the protein from a native to a denatured conformation. Overall, the results suggest that the solution-phase secondary structures of A-

state ubiquitin are conserved in the gas phase. This method also provides sufficient sensitivity to differentiate between two gas-phase conformers of the same charge state with subtle structural variations.

INTRODUCTION

Tertiary structures of proteins are associated with the biological functions determined by the physicochemical interactions between the proteins and other biomolecules.[1] Significant structural disruption of a protein can lead to loss of functionalities and can be detrimental to human health. For instance, disrupting the normal tertiary structure of amyloid proteins in Alzheimer's disease, a protein-misfolding disease, leads to loss of function, aggregation, and brain toxicity.[2] Accurate determination of protein tertiary structures is therefore critical to understanding the biological mechanisms of disease progressions.

Protein structures can be determined via various structural biology modalities,[3] ranging from conventional, high-resolution tools such as CryoEM,[4-6] NMR[7, 8] and X-ray crystallography[9, 10] to low-resolution mass spectrometry-based methods.[11, 12] Various mass spectrometric approaches, such as chemical labeling, photoaffinity labeling, and hydrogen-deuterium exchange (HDX)-MS,[13-15] along with gas-phase dissociation methods including electron-capture dissociation (ECD) [16-19] and ultraviolet photodissociation (UVPD),[20-22] afford lower structural resolution but superior sensitivity compared to the atomic-resolution NMR and X-ray crystallography.[11, 12] For example, top-down protein cross-linking mass spectrometry (XL-MS) enables the deduction of local secondary structures as well as general topologies of proteins via the distance constraints imposed by cross-linkers.[23-28] The protein cross-linking reaction is typically performed in solution, followed by gas-phase tandem mass spectrometry

(MS^n, where n > 1) fragmentation of the modified protein to localize the linker attachments.[23-28] The cross-linking reaction, however, can alternatively be performed in the gas phase via ion/ion reactions between multiply charged protein cations and singly charged cross-linker anions.[29-31] For example, the McLuckey group used ubiquitin cations and ethylene glycol bis(sulfosuccinimidyl succinate) (sulfo-EGS) cross-linker anions to first develop a gas-phase XL-MS workflow.[29] The reactant ions with opposite charges were mutually confined in a radio frequency (RF) ion trap to effect a cross-linking reaction. Briefly, the oppositely charged ions form a long-lived, electrostatic complex that initiates a covalent cross-linking reaction.[32] Collision-induced dissociation (CID) then produces fragment ions, both covalently modified and unmodified, which can be used to locate cross-linking sites.[29] The Coulombic attraction between the oppositely charged ions[33-35] results in significantly reduced reaction times for the gas-phase ion/ion cross-linking reactions compared to in-solution analogues (*i.e.*, milliseconds to seconds[29-32, 36, 37] versus minutes to hours,[23, 38-40] respectively). The gas-phase approach also provides a high degree of control over the reactant species and relative abundances and enables the investigation of gas-phase protein structures.

The accuracy of tertiary structures obtained from a gas-phase top-down XL-MS is dependent on the preservation of the solution structure during ionization, ion transfer between ion optics, and/or storage of oppositely charged reactant ions in an RF-confined ion trap. Obtaining sufficient structural resolution with gas-phase XL-MS to validate the conservation of solution protein structure, however, is challenging due to several technical limitations.[29] First, using singly deprotonated sulfo-EGS cross-linker anions, $[\text{sulfo-EGS} - \text{H}]^-$, limits target linker sites to neutral amine groups of basic amino acid residues and thus no cross-linking reactions occur at protonated residues.[29] By introducing singly sodiated sulfo-EGS cross-linkers herein,

[sulfo-EGS – 2H + Na]$^-$, gas-phase sodium-proton exchange can occur at those protonated residues, enhancing the reactivity towards sulfo-NHS chemistry.[41] As a result, this approach explores three covalent modification sites, namely neutral primary amines, positively charged ammonium and guanidinium groups, increasing the number of available cross-linking sites to provide enhanced topology mapping abilities. The second technical limitation is the ambiguity in the localization of sites of linker attachment when analyzing only b-/y-type terminal MS^2 fragment ions.[23, 29] Mass-selective MS^3 of MS^2 fragment ions of interest may alleviate the ambiguity, although this requires additional experimental time and further dilutes product ion signals.[23, 29] Alternatively, internal (or secondary) fragment ions can be generated and analyzed at the MS^2 level, which reduces experimental time.[42-44] Several research groups have recently demonstrated that analyzing internal fragment ions, in addition to terminal counterparts, enhances the identification of naturally occurring disulfide cross-linking positions in proteins.[45, 46] This finding suggests that analyzing covalently modified internal fragment ions could improve localization of the sulfo-EGS cross-linking sites in gas-phase XL-MS.

Herein, we present a modified gas-phase XL-MS approach that reveals improved structural information of alcohol-denatured, A-state ubiquitin.[29] Singly sodiated sulfo-EGS cross-linker anions are used as ion/ion reaction reagents and both terminal and internal fragment ions produced via IRMPD are used for the assessment of covalent linkage sites. This modified workflow enables covalent cross-linking at N-terminus, lysine, and arginine residues, regardless of their protonation state, while allowing for a more unambiguous identification of cross-linking sites. Atomistic molecular dynamics (MD) simulations accelerated by the temperature replica exchange protocol[47] are used to simulate the gas-phase conformation of the denatured ubiquitin. The combined experimental and simulated data suggest that the A-state conformation is

conserved from the solution phase to the gas phase, retaining its characteristic secondary motifs for over 1,500 ms during the ion/ion reaction time.

EXPERIMENTAL

I. Materials

Ubiquitin from bovine erythrocytes and the matrix-assisted laser desorption/ionization (MALDI) matrix α-cyano-4-hydroxycinnamic acid (CHCA) were purchased from Sigma-Aldrich (St. Louis, MO, USA). Cross-linking reagent sulfo-EGS was purchased from Thermo Scientific (Rockford, IL, USA). HPLC-grade methanol was purchased from Fisher Chemical (Waltham, MA, USA). Zip Tips® with strong cation exchange resins (ZTSCX) were purchased from EMD Millipore Corporation (Billerica MA, USA). Ubiquitin was used without further purification and an electrospray ionization (ESI) solution was prepared at a final concentration of 10 μM in 49.5/49.5/1 (v/v/v) methanol/water/acetic acid. ZTSCX was conditioned by aspirating and discarding 18 MΩ water 5 times. An aqueous solution of 10 mM sulfo-EGS in distilled water was then pipetted up and down 20 times to remove sodium ions. A sulfo-EGS solution that was either filtered or unfiltered was mixed with a saturated methanol solution of the CHCA matrix in a 1:1 ratio to generate $[\text{sulfo-EGS} - \text{H}]^-$ or $[\text{sulfo-EGS} - 2\text{H} + \text{Na}]^-$ ions, respectively, upon MALDI. Two layers of 1 μL of the mixture were manually spotted onto an MTP AnchorChip MALDI target plate (Bruker Daltonics, Billerica, MA, USA).

II. Instrumentation

All the experiments were performed on a 7T solariX XR Fourier transform ion cyclotron resonance (FT-ICR) mass spectrometer equipped with an Apollo II dual MALDI/ESI source

and a dynamically harmonized ParaCell (Bruker Daltonics, Billerica, MA, USA). The MALDI source employs a Smartbeam II Nd:YAG laser system (2 kHz, 355 nm). The sulfo-EGS cross-linker anions were generated via MALDI (3,000 laser shots at 2 kHz) and the ubiquitin protein cations were generated via ESI (120 µL/h spray flow rate with a 4.0 kV spray voltage at 100 °C drying gas temperature). Data were collected from *m/z* 200 to *m/z* 5,000 using a 0.9787-second time-domain transient length, resulting in a mass resolving power of ~50,000 at *m/z* 1,000. Data were visualized using Compass DataAnalysis 5.0 (Bruker Daltonics, Billerica, MA, USA).

Generating abundant internal fragment ions from covalently modified proteins when performing gas-phase XL-MS is not readily achieved using existing hardware on the FT-ICR mass spectrometer. Intact protein ions are first introduced into the hexapole through the funnel-skimmer region, where they undergo ion/ion reactions with cross-linker reagents, before being fragmented downstream in the ICR cell. However, infrared multiphoton dissociation (IRMPD) in the ICR cell is better suited to produce sufficient, modified internal fragment peptide ions relative to sustained off-resonance irradiation (SORI) CID due to higher fragmentation efficiency.[48] To enable this, A Synrad Duo Lase 50 W continuous wave CO_2 laser (J48-5W; Synrad, Mukilteo, WA, USA) was interfaced to the rear of the ICR magnet bore, as described previously.[49] Briefly, the laser beam (10.6 µm wavelength) was introduced into the ICR cell through a barium fluoride (BaF_2) window. The laser power was adjusted to 40 – 50 % via a UC-1000 laser controller (Synrad, Mukilteo, WA, USA) and the irradiation time was modulated from 0.6 – 1.0 sec using the ftmsControl software (Bruker Daltonics, Billerica, MA, USA). IRMPD also achieves a high signal-to-noise ratio (SNR) by enabling averaging of multiple spectra without requiring a gas pulse between scans, resulting in improved speed compared to

SORI CID.[49] Achieving a high SNR of informative fragment ions is critical for accurately identifying cross-linking sites.

ECD was performed to determine the locations of protonation and salt bridges in ubiquitin, using the following parameters: 2.0 VDC ECD bias, 30 VDC ECD lens, and 0.020 seconds electron beam irradiation time. A total of 40 spectra were averaged to improve the signal-to-noise ratio, and three replicates were collected. The ECD fragment ions were assigned based on ProteinProspector data base.[50]

III. Ion/Ion Reactions

Gas-phase cross-linking ion/ion reactions were performed via software modifications to the existing electron transfer dissociation (ETD) capability of the commercial FT-ICR MS (**Figure 1**).[49, 51-55] Briefly, MALDI-generated sulfo-EGS cross-linker anions (1 second) and ESI-generated multiply charged ubiquitin cations ($[M + 8H]^{8+}$) (500 milliseconds) were sequentially isolated via the quadrupole mass filter (QMF) and injected into the hexapole ion trap (**Figure 1a and 1b**). A mutual storage ion/ion reaction period (1,500 ms) of the oppositely charged reactant ions produced long-lived, charge-reduced, electrostatic complex cations with varying numbers of cross-linkers attached (**Figure 1c**). After the ion/ion reactions, the residual ubiquitin precursor ions and electrostatic complex ions were transferred to the ICR cell, where the target complex with a single cross-linker attached was subsequently isolated using a frequency sweep isolation method (**Figure 1d**). The electrostatic complex ions were then covalently cross-linked via IRMPD, signified by the consecutive losses of two sulfo-NHS moieties (**Figure 1e**). Excess energy from the IR laser also provided for subsequent fragmentation of covalently modified ubiquitin (**Figure 1e**). The total IR laser irradiation time

varied from 0.6 to 1.0 seconds per spectrum, and 60 spectra were averaged. The IRMPD fragment ions were then analyzed to determine the cross-linking sites on ubiquitin. Internal calibration was performed post-acquisition using abundant b-/y-type fragment ions (y_{12}^{2+} at *m/z* 661.407, y_{18}^{2+} at *m/z* 1049.100, y_{12}^{+} at *m/z* 1321.806, b_{18}^{+} at *m/z* 2033.135) from acquired IRMPD spectra of unmodified and modified ubiquitin (acceptable mass accuracy thresholds less than 5.0 ppm). IRMPD fragment ions were assigned based on ProteinProspector data base.[50]

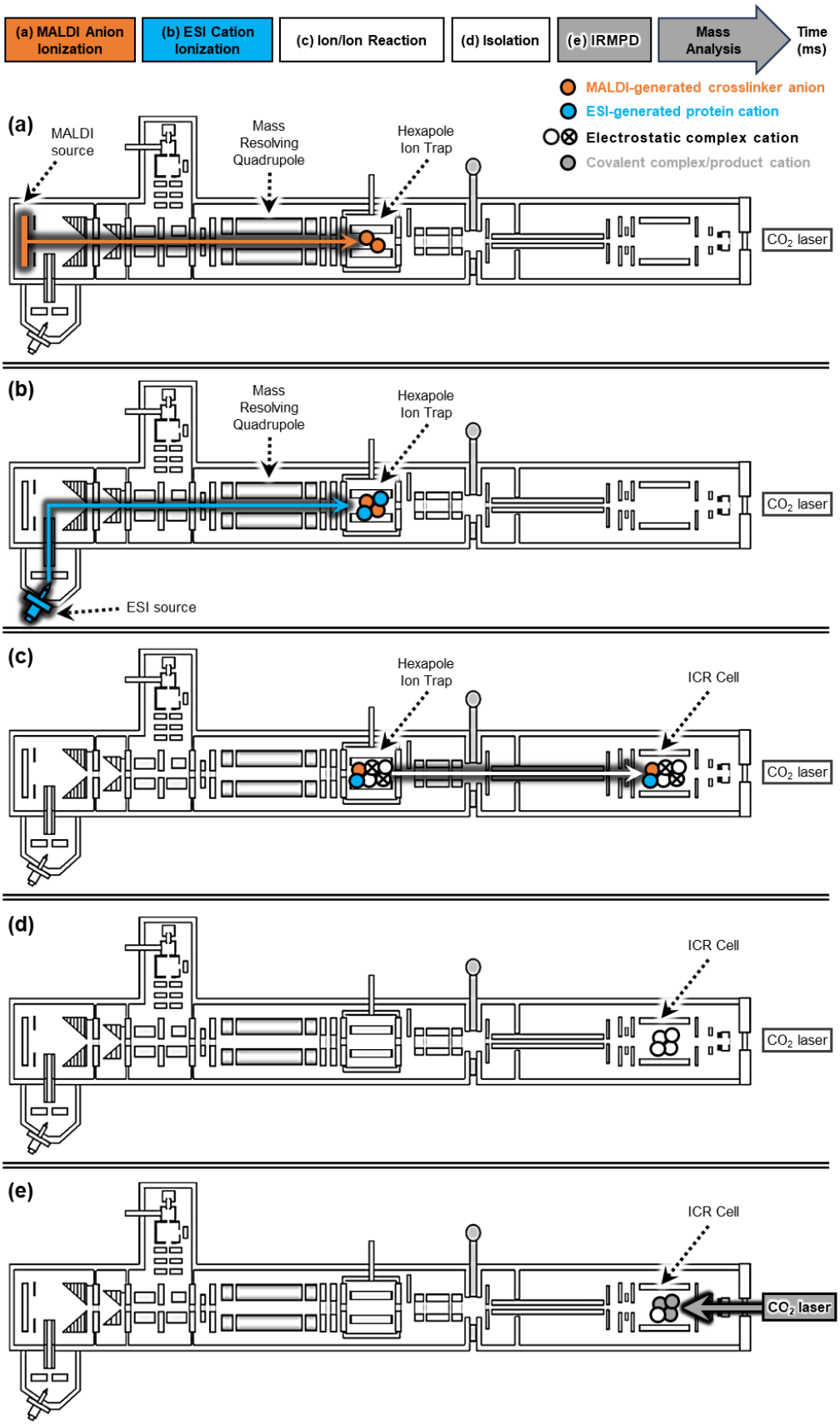

Figure 1. Workflow for gas-phase cross-linking of protein via ion/ion reactions starts with (a) injection and isolation of MALDI-generated singly charged cross-linker anions (●) followed by (b) ESI-generated multiply charged protein cations (●). (c) Mutual storage of the oppositely charged reactant ions in the hexapole ion trap forms electrostatic complex cations containing either a single cross-linker (○) or multiple cross-linkers (⊗). The complex and residual precursor cations are transferred to the ICR cell for (d) isolation of the electrostatic complex with a single cross-linker attached (○) and (e) IRMPD of this electrostatic complex to produce a covalently modified protein (●) as well as sequence-informative fragments.

V. Computational Modeling

A-state ubiquitin[56-58] was generated from the primary amino acid sequence by using the gbNeck2 implicit solvent model[59, 60] and ff14SBside protein force field[61-63] within the Bayesian inference-based modeling employing limited data (MELD)[64, 65] replica exchange molecular dynamics (REMD) framework.[47] To encourage the alcohol-denatured conformations,[56-58] certain restrictions were placed on three primary secondary structures: the N-terminal β-hairpin, the first α-helix at residues 23 through 34, and the second α-helix at residues 40 through 74. The α carbons across the second α-helix were kept at a minimum distance of 45 Å from each other. This initial MELD × MD simulation was run for 0.5 microseconds. Then, CPPTRAJ[66] was used to cluster the ensemble by structural similarity using hierarchical clustering. The starting conformation for downstream MD simulations was selected as the centroid of the most populated cluster.

A total of eight positive charges were evenly distributed across the starting conformation of A-state ubiquitin in its neutral, non-zwitterionic state, taking into consideration the multiple charging of biopolymer ions during the ESI process.[67] The scaling factor between 0 to +1 for residue charges was derived using the AMBER package[68] for each atom that makes up the potential charge-bearing amino acid residues; arginine (4x), lysine (7x), histidine (1x), and N-terminal methionine. Atomic charges were then adjusted using the derived scaling factor. The

final charge of 8+ ubiquitin was then divided by the total 13+ charge, giving the initial A-state conformational model.

The ff14SBside protein force field was used to simulate the initial 8+ A-state conformation for 2.5 microseconds in a vacuum.[61-63] REMD[47] was incorporated into MD simulation with 16 replicas spreading across the temperatures between 300 K and 400 K to improve phase space sampling. Hierarchical clustering was then applied to the ensemble structures at 300 K to select representative cluster centroids. Collidoscope, a recently developed open-source tool, was used to calculate the collision cross sections (CCSs) of the final structures.[69] Native and denatured ubiquitin structures obtained from the protein data bank (PDB) or MD simulation were visualized using PyMOL software (The PyMOL Molecular Graphics System, Version 1.2r3pre, Schrödinger, LLC.).

RESULTS

The 8+ charge state of ubiquitin was selected here to demonstrate a proof-of-concept for this method (**Scheme 1**) for several reasons. The conformational stability of a protein is critical for confirming that the structure remains consistent during ion/ion reactions that last for hundreds of milliseconds in the gas phase. The gas-phase conformation of alcohol-denatured 8+ ubiquitin has previously been shown to be stable over 1 second of storage time in an ion trap.[70] This charge state of ubiquitin has shown two major conformations, which simplifies XL-MS data analysis compared to searching a large number of protein conformations.[70] By comparison, 7+ ubiquitin may contain up to five conformations.[70] Although 6+ ubiquitin remains stable in two main conformers over 1 second of storage time in an ion trap,[70] it was not selected due to less efficient IRMPD fragmentation compared to 8+ ubiquitin.[71]

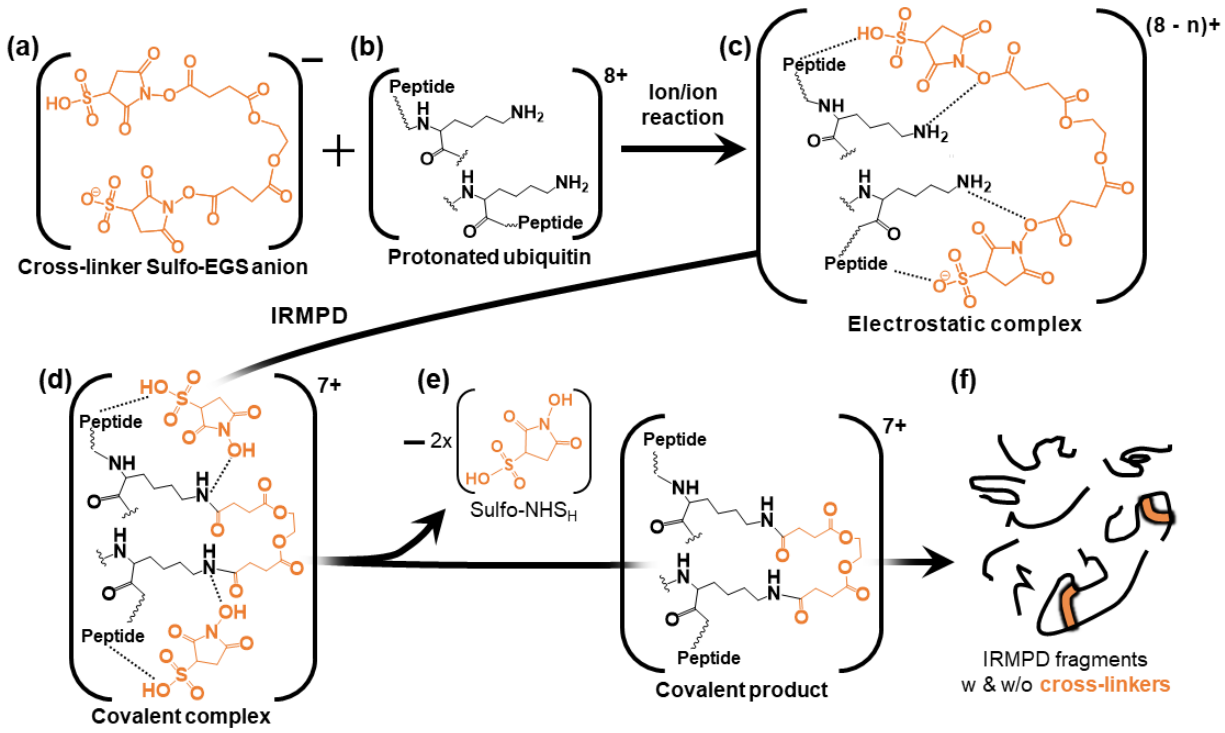

Scheme 1. Gas-phase ion/ion cross-linking between (a) a cross-linker [sulfo-EGS – H]$^-$ anion and (b) a ubiquitin [M + 8H]$^{8+}$ cation forms (c) electrostatic complex cations (n=1, 2, 3…). (d, e) IRMPD on the isolated [M + 8H + (sulfo-EGS – H)]$^{7+}$ complex cation drives a covalent modification reaction, which is signified by the loss of two neutral sulfo-NHS$_H$ moieties. (f) Further IR laser irradiation fragments the covalently cross-linked ubiquitin.

I. XL-MS Using [sulfo-EGS – H]$^-$

Singly deprotonated sulfo-EGS cross-linker anions, [sulfo-EGS – H]$^-$, can be used to covalently modify 8+ ubiquitin at neutral amine groups of basic amino acid residues such as lysine and arginine, leading to restricted modification sites. Briefly, singly deprotonated sulfo-EGS anions (**Figure 2a**) were stored with 8+ ubiquitin cations (**Figure 2b**), forming the long-lived, electrostatic complexes with varying numbers of cross-linkers attached (**Figure 2c**). The sequential addition of nominal mass 615 Da to the precursor ubiquitin cations indicates the

attachment of each [suflo-EGS – H]$^-$ anion. Numerous fragment ions with and without covalent modifications were produced by IRMPD of the electrostatic complex with a single cross-linker attachment (**Figure 2d**). Covalent cross-linking, signified by the consecutive loss of two sulfo-NHS_H moieties from $[M + 8H + \Delta]^{7+}$, is enabled via IRMPD (**Figure 2e**). Analysis of the XL ubiquitin fragment ion spectrum produced via IRMPD enables identification of the cross-linked amino acid residues, which can be used to infer protein structure. For example, modified b_{18}, b_{32}, and b_{39} fragment ions are not detected (**Figure 2f**), indicating no cross-linking is present on the N-terminal portion of the protein (*e.g.*, between M1, K6, K11, K27, K29, and K33). The absence of a modified b_{52} fragment ion, along with the presence of a modified b_{58} fragment ion and the presence of a modified internal fragment ion $[^{33}KEGIPPDQQ^{42}RLIFAG^{48}KQLEDG^{54}RTLSD]^{2+}$ (**Figures 2f**), suggests cross-linking between K33–R54, R42–R54, or K48–R54. However, cross-linking with K33 or R42 is unlikely because the distances from R54 in the A-state structure exceeds the 16.1 Å length of the cross-linker (**Figure 3**). It is then likely that K48–R54 is cross-linked, which suggests that the K48 and R54 residues are not protonated in the gas phase.[41] A comparison of fragment ion masses, corresponding mass accuracies, and measured isotopic distributions between unmodified $[M + 7H]^{7+}$ ubiquitin and modified $[M + 8H + \Delta]^{7+}$ ubiquitin is used to facilitate accurate fragment ion assignments (**Supplemental Figures S1-S3**).

Though only a single cross-link is present in the singly modified protein, it is likely that an ensemble of multiple cross-linked positions is present in the modified protein ion population. Additional cross-linking is indicated at K63–R72 or K63–R74 by the presence of a modified y_{18} fragment ion and the absence of a modified y_{12} (**Figures 2f**). The presence of c_{75}^{7+} and z_3^+ and absence of z_1^+ and z_2^+ fragment ions in the ECD analysis of alcohol-denatured 8+ ubiquitin

suggests R74 is a site of protonation (**Supplemental Figure S4**), indicating K63–R72 is the correct cross-linking assignment. Additionally, gas-phase compaction of the basic residues and potential salt bridge formation with neighboring acidic residues bring K63 and R72 close to one another and enable cross-linking (*vide infra*). In either case, the intra-protein distance between K63 and either R72 or R74 in the native conformation is much greater than the length of the cross-linker. However, a significant decrease in the inter-residue distance for ubiquitin is possible via a structural transition to the A-state[56-58] (**Figure 3**). Therefore, the K63–R72 or K63–R74 covalent modification reflects a transformation of the C-terminal beta-sheets in native ubiquitin to the C-terminal alpha-helix in A-state ubiquitin.

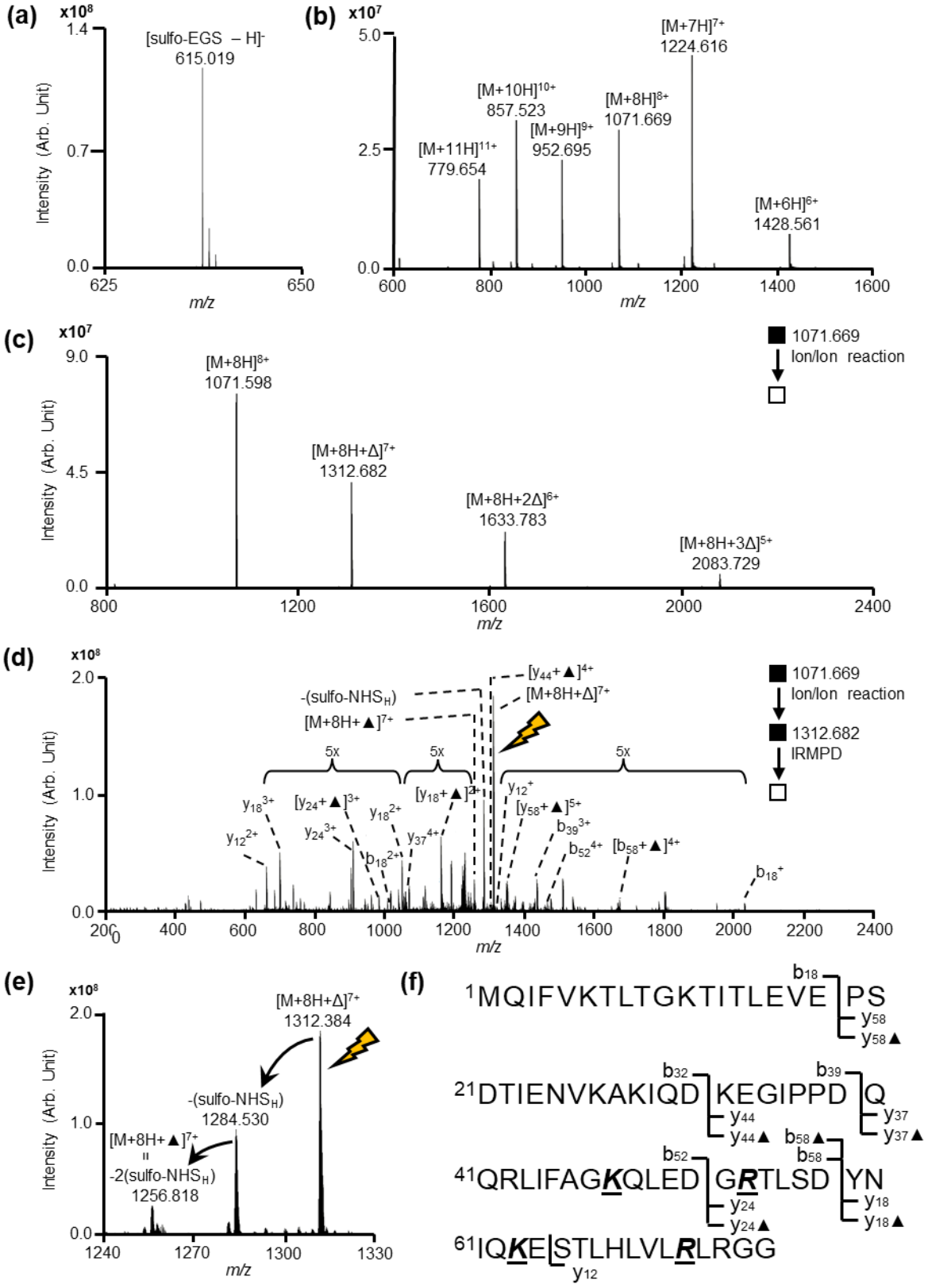

Figure 2. (a) MALDI-generated, singly charged sulfo-EGS cross-linker anions and (b) ESI-generated multiply charged ubiquitin cations are used in (c) a gas-phase ion/ion reaction between $[\text{sulfo-EGS} - \text{H}]^-$ and $[\text{M} + 8\text{H}]^{8+}$ that forms electrostatic complex cations with varying numbers of $[\text{sulfo-EGS} - \text{H}]^-$ attachment (denoted by Δ). (d) IRMPD (1 s and 50 % power) of isolated $[\text{M} + 8\text{H} + \Delta]^{7+}$ drives covalent modifications and subsequently fragments the covalently cross-linked ubiquitin. (e) Magnification of the relevant mass range shows consecutive losses of two sulfo-NHS_H moieties from $[\text{M} + 8\text{H} + \Delta]^{7+}$ upon IRMPD (where ▲ = $\Delta - 2(\text{sulfo-NHS}_\text{H})$), signifying covalent modifications. (f) Significant b-/y-type fragment ions are observed. The bolded, underlined, and italicized residues indicate cross-linking sites. Note: Squares indicate positive ion mode analysis, filled squares represent ion isolation events, and hollow squares represent full scan acquisition. The thunderbolt indicates IRMPD.

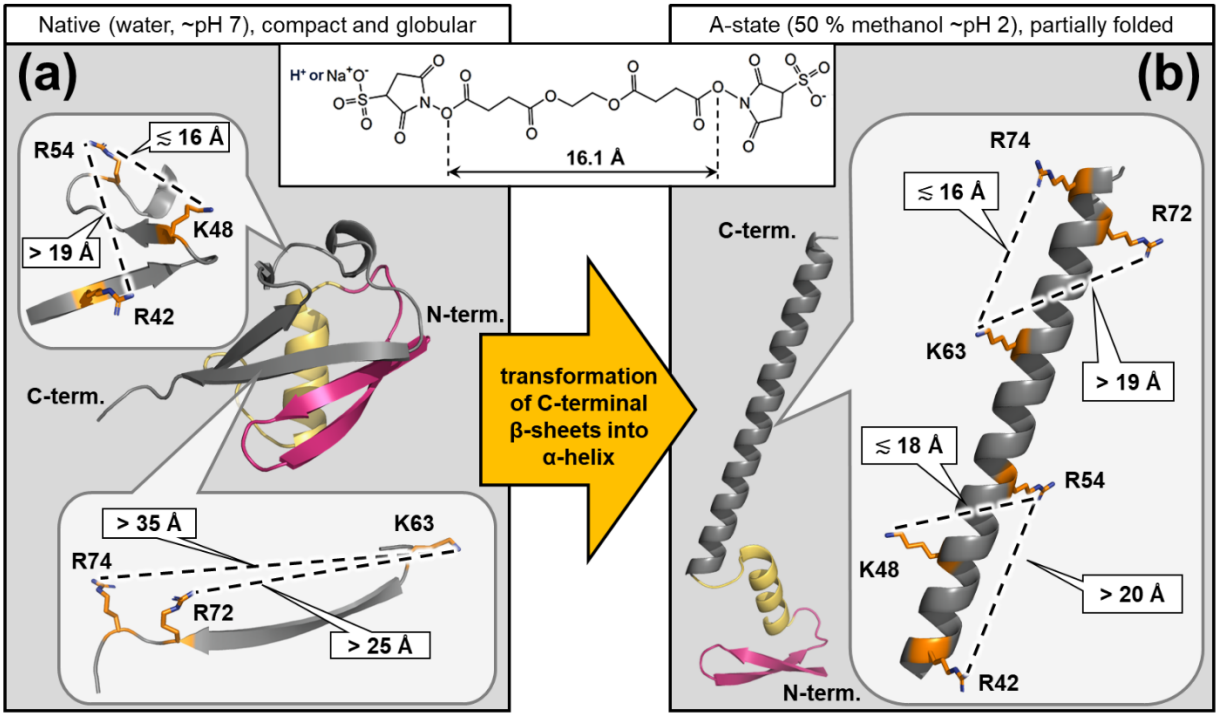

Figure 3. Through-space distances between C-terminal basic residues on (a) the crystal structure of native ubiquitin (PDB ID: 1UBQ) and (b) the solution structure of A-state ubiquitin based on NMR structures (built from (a) using PyMOL).

II. XL-MS Using [sulfo-EGS – 2H + Na]⁻

The use of the $[\text{sulfo-EGS} - \text{H}]^-$ reagent limits cross-linking to non-protonated, neutral lysine and arginine residues, as demonstrated above. Alternatively, singly sodiated sulfo-EGS cross-linkers, $[\text{sulfo-EGS} - 2\text{H} + \text{Na}]^-$ can be used to react at any basic residue regardless of

protonation.[41] IRMPD spectra are analyzed in a similar manner to gas-phase XL-MS with [sulfo-EGS – H]$^-$ (**Figure 4** and **Supplemental Figures S5-S7**). For example, the absence of a modified b_{18} fragment ion and the presence of a modified b_{32} fragment ion may suggest cross-linking at K27–K29 (**Figures 4c**).[29] However, more conservatively, cross-linking between any combination of M1, K6, K11, K27, and K29 (but not M1, K6, and K11) is possible. The presence of a modified b_{39} fragment ion expands these combinations to also involve K33 (**Figure 4c**). Relying only on the terminal b-type fragment ions is thus insufficient to determine the exact site of linker attachment. Conversely, cross-linking at K27–K29 (inter-residue distance < 12 Å) is definitively assigned by identification of a modified internal fragment ion [TIENV^{27}KA^{29}KIQD]$^+$ (**Supplemental Figure S7**). Detection of interpeptide cross-links (*e.g.*, by disulfide bonds[45, 46] or by sulfo-NHS-based cross-linking reagents[26, 72]) also enhances localization of covalent modifications on residues that are distant from each other along the backbone. Four additional cross-linking sites, M1–K29, M1–K33, K6–K29, and K6–K33, are assigned by identification of the modified internal fragment ion [^{1}MQIFV^{6}KTLTG /==/ A^{29}KIQD^{33}KEGI]$^{2+}$, where /==/ indicating interpeptide cross-linking (**Supplemental Figure S7**). Non-canonical cleavage C-terminal to G residues[42, 43] and C-terminal to K residues[42] in CID-induced internal fragment ions has been observed previously, supporting the identification of this interpeptide cross-link based on the accurate mass (**Supplemental Figure S7**). These four potential cross-linking sites suggest high spatial proximity between the N-terminal beta-hairpin and alpha-helix spanning from I23 through E33. The two C-terminal cross-linking sites, K48–R54 and K63–R72, are determined in the same manner as for the ion/ion reactions using [sulfo-EGS – H]$^-$ (**Figure 4c** and **Supplemental Figures S5-S7**).

The use of [sulfo-EGS – 2H + Na]$^-$ introduces cross-linking in the N-terminal half of A-state ubiquitin that is not observed when using [sulfo-EGS – H]$^-$ as the reagent ion type (**Table 1**). This is likely due to the fact that protonation of a target amine group results in a lack of nucleophilic reactivity towards sulfo-NHS chemistry with the [sulfo-EGS – H]$^-$ reagent.[41] Additionally, the potential presence of a strong, gas-phase salt bridge network with neighboring carboxylic amino acid residues in the N-terminal region can sterically shield the target amine groups. However, sodium cations introduced by [sulfo-EGS – 2H + Na]$^-$ alter gas-phase cross-linking reactivities via gas-phase exchange with protonated basic residues[41] or via strong salt bridge network participants. Relatively low affinity of the basic residues towards sodium compared to a proton enhances the nucleophilicity of the ammonium and guanidinium groups, enabling nucleophilic attack on the ester-carbon of sulfo-EGS cross-linker and thus covalent modification.[41] The retention of sodium during covalent modification and fragmentation induced by IRMPD confirms gas-phase metal transfer from the cross-linker anion to the protonated ubiquitin cation (**Figure 4a** and **Supplemental Figure S5**). Interestingly, b_{32}, b_{39}, b_{52}, b_{58}, and y_{58} fragment ions retain sodium, while y_{24}, y_{37}, and y_{44} fragment ions do not. We also note a roughly 9-fold higher intensity of the modified y_{18} fragment ion that does not retain sodium compared to the modified y_{18} that retains sodium (**Supplemental Figure S6**). This observation suggests that sodium plays a critical role in the covalent cross-linking of the N-terminal half of A-state ubiquitin.

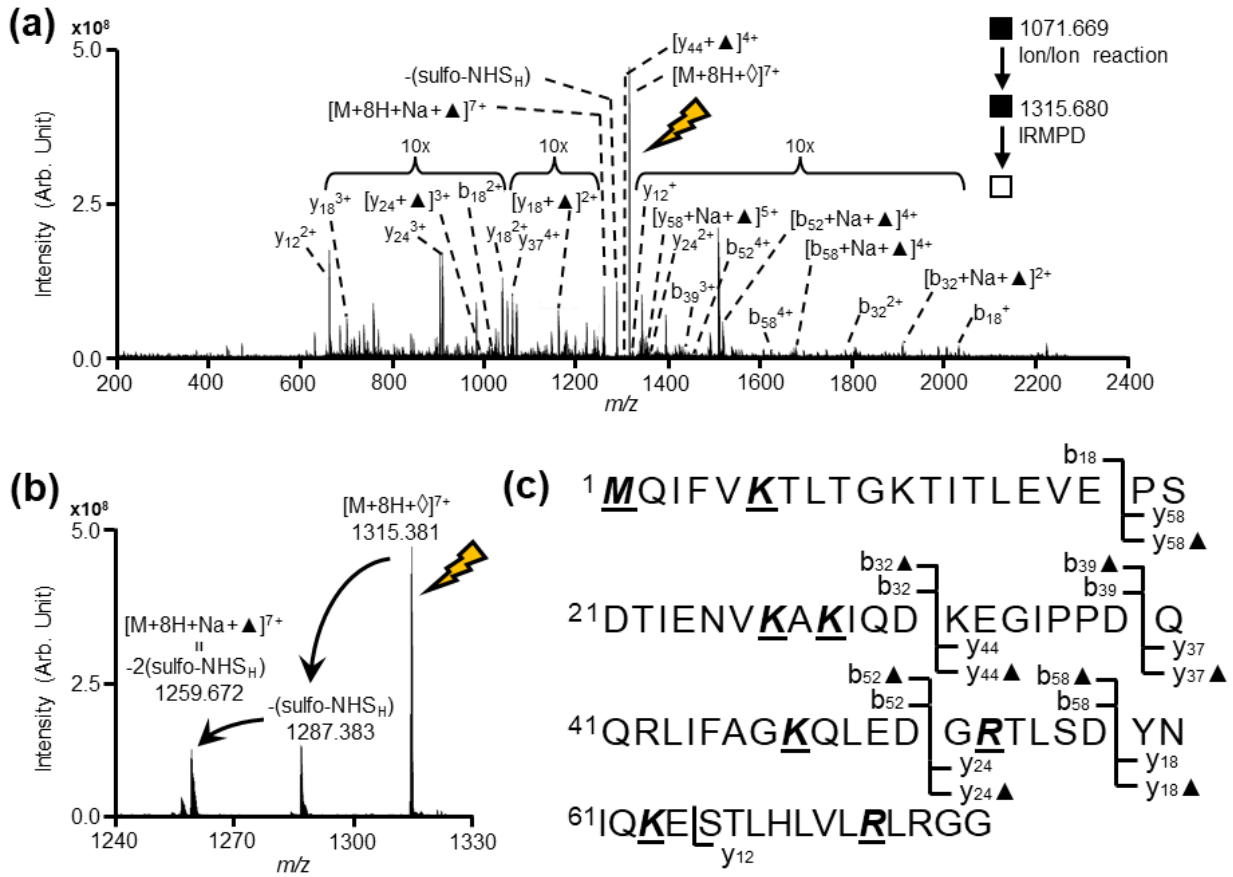

Figure 4. Gas-phase ion/ion reaction between $[\text{sulfo-EGS} - 2\text{H} + \text{Na}]^-$ and $[\text{M} + 8\text{H}]^{8+}$ forms electrostatic complex cations with varying numbers of $[\text{sulfo-EGS} - 2\text{H} + \text{Na}]^-$ attachment (◊). (a) IRMPD (0.6 s and 40 % power) of isolated $[\text{M} + 8\text{H} + ◊]^{7+}$ drives covalent modifications and subsequently fragments the covalently cross-linked ubiquitin. (b) Magnification of the relevant mass range shows the consecutive losses of two sulfo-NHS_H moieties from $[\text{M} + 8\text{H} + ◊]^{7+}$ via IRMPD (where ▲ = ◊ – 2(sulfo-NHS_H – Na)), signifying the covalent modifications. (c) Significant b-/y-type fragment ions are observed. The bolded, underlined, and italicized residues indicate cross-linking sites. Note: The thunderbolt indicates IRMPD, squares indicate positive ion mode analysis, filled squares represent ion isolation events, and hollow squares represent full scan acquisition.

Table 1. Modified terminal and internal fragment ions associated with assigned cross-linking sites are summarized with respect to $[\text{sulfo-EGS} - \text{H}]^-$ versus $[\text{sulfo-EGS} - 2\text{H} + \text{Na}]^-$. Red Xs denote the absence of a detected fragment ion and blue checks denote the presence of a detected fragment ion.

Fragment ions	$[\text{sulfo-EGS} - \text{H}]^-$	$[\text{sulfo-EGS} - 2\text{H} + \text{Na}]^-$	Cross-linking site
b_{32}▲, b_{39}▲	X	✓	Undetermined
[TIENV^{27}**K**A^{29}**K**IQD + ▲]$^{2+}$	X	✓	K27-K29
[^{1}**M**QIFV^{6}**K**TLTG/==/A^{29}**K**IQD^{33}KEGI + ▲]$^{2+}$	X	✓	M1-K29 K6-K29
b_{52}▲	X	✓	Undetermined
b_{58}▲, y_{37}▲, y_{44}▲	✓	✓	K48-R54
[^{33}KEGIPPDQQ^{42}RLIFAG^{48}**K**QLEDG^{54}**R**TLSD + ▲]$^{2+}$	✓	✓	
y_{18}▲, y_{12}	✓	✓	K63-R72

III. Molecular Dynamics Modeling

When simulating gas-phase protein ions generated via ESI, the charge or protonation sites on the starting structure are crucial factors. This is because the presence of zwitterionic salt bridges and Coulombic repulsion on the protein ion can directly impact the outcome of the structural prediction.[31, 73] In this study, the charges are computationally evenly distributed throughout the protein because unambiguous determination of the charge sites is difficult both experimentally and theoretically.[74] Non-ergodic fragmentation methods such as ECD[30] and UVPD[75] produce complex fragmentation profiles from charge isomers, which can complicate identifying charge sites. Therefore, we utilized ECD analysis here only for identifying partial charge locations and validating salt bridges indicated by the simulated structures (**Supplemental Figure S4**).

An ensemble of conformations is generated via the MD simulation (**Figure 5a**), and conformers presenting good agreement with XL-MS data are selected for visualization (**Figure 5** and **Figure 6**). The simulated conformers show conservation of three major secondary structures in solution-phase A-state ubiquitin, namely an N-terminal beta-hairpin as well as two alpha-helices spanning from I23 through E33 and from Q40 through R74. A well conserved N-terminal beta-hairpin motif would allow cross-linking at K6–K11 given the shorter distance

between the two residues in the native structure (~14 Å). However, the lack of observed cross-linking in this region can be attributed to steric hindrance around K11, which is partially caused by the salt bridge formation between K11 and E34 residues (**Figures 5c, 6b**). ECD fragment ion z_{66}^{6+} with partial fractional abundance also suggests participation of K11 in a salt bridge (**Supplemental Figure S4).**

The experimental gas-phase XL-MS data above are insufficient to narrow down the amino acid residues paired at the cross-linking site M1/K6–K29/K33. While it is unclear whether M1, K6, or K33 are protonated based on the ECD experiments, a small portion of conformers appears to be protonated at K29 (**Supplemental Figure S4**). A simulated conformer shows the burial of K29 residue by neighboring residues E16 and D21, forming a compact local structure via a salt bridge network that blocks access to K29 by [sulfo-EGS – H]$^-$ (**Figure 5d**). Sodium cations likely disrupt these non-covalent interactions, enabling covalent cross-linking at M1/K6–K29 via [sulfo-EGS – 2H + Na]$^-$. It is possible that certain compact conformers may alleviate the structural constraints in the N-terminal half, leading to the exposure of the protonated K29 (**Figure 6c**). This again results in no cross-linking at K27–K29 via [sulfo-EGS – H]$^-$ (**Table 1**) due to the ammonium group's lack of reactivity towards NHS chemistry.[41] Sodium cations from the singly sodiated sulfo-EGS anions, again, enable K27–K29 cross-linking by altering the gas-phase chemistry.[41] Therefore, the cross-linking at K27–K29 and M1/K6–K29 indicate the presence of two conformers with CCS values of 1772.86 Å^2 and 1834.89 Å^2, respectively.

The simulated structures also indicate gas-phase compaction of K48, R54, and K63 residues, forming salt bridges with D52, E51, and E64, respectively. ECD fragment ions c_{51}^{5+}, z_{25}^{3+}, and z_{23}^{3+} with partial fractional abundances also suggest participation of E51, D52, and

R54 in salt bridges (**Supplemental Figure S4**), supporting the simulated data. These non-covalent interactions bring the sidechains of K48 and R54 to within 10 Å and bring the sidechains of K63 and R72 to within 16 Å, which is within reach of the cross-linker (**Figures 5e** and **5f**). This further supports experimentally determined cross-linking sites at K48–R54 and K63–R72.

Both MD simulations and experimental XL-MS data indicate that the solution-phase secondary structures of A-state ubiquitin are conserved in the gas phase, while the N-terminal half of the protein is in a more compact conformation in the gas phase (**Figure 5b** and **Figure 6a**). We note that the three major secondary structures rotate freely with respect to the loops that separate them in the solution (**Figure 3**).[56-58] This small difference between the solution-phase and gas-phase structures is likely due to the formation of a salt bridge network in the gas phase (**Figures 5c, 5d** and **Figures 6b, 6c**), which is replaced by water solvation in the solution phase. The two conformers that are simulated and discussed above show good agreement with the experimental XL-MS data. The sum intensities of all the isotopes of the two internal fragment ions associated with cross-linking sites K27–K29 and M1/K6–K29 (**Supplemental Figure 7**) show that the conformer with a CCS value of 1834.89 $Å^2$ is approximately 12-fold more abundant compared to the other conformer with a CCS value of 1772.86 $Å^2$(**Supplemental Figure S8**). The absolute CCS values calculated here are not intended to be highly accurate and we note that different values may be obtained using other CCS prediction tools. However, the relative differences in CCS values between the two conformers are reliable and previous ion mobility mass spectrometry (IM-MS) reports also support these findings, showing a major conformer present at higher CCS and a minor conformer at lower CCS.[70]

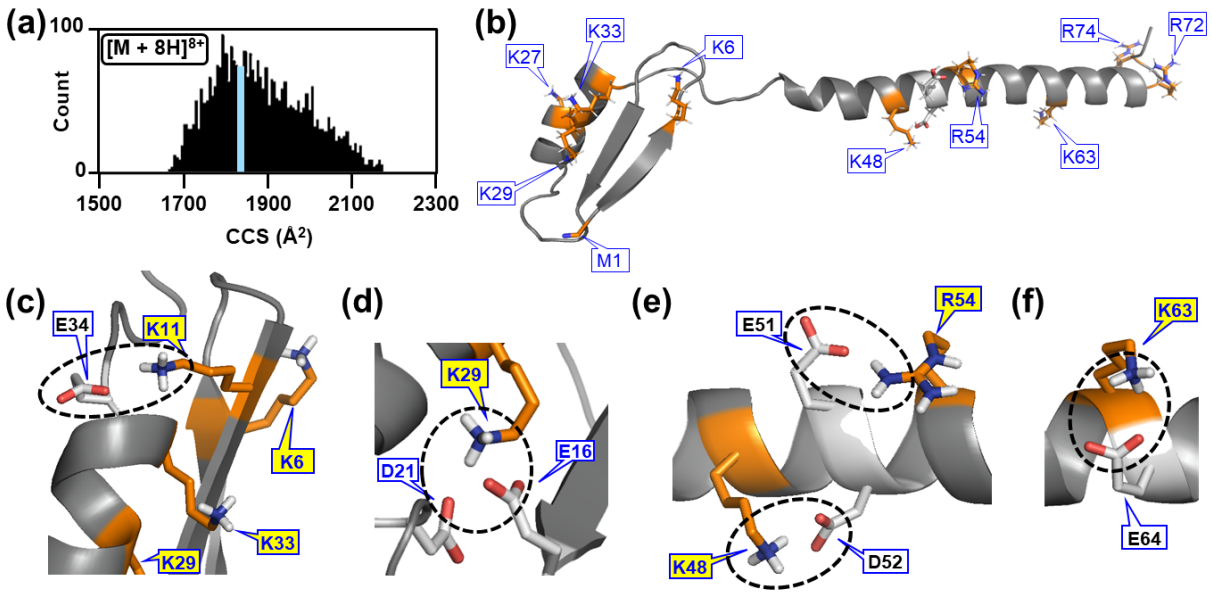

Figure 5. (a) The number of MD-simulated 8+ ubiquitin ensemble structures are plotted against collision cross-sections predicted via Collidoscope. (b) A selected conformer from at CCS = 1834.89 Å^2 (turquoise vertical line in panel 5a) highlights the basic residues of interest. Local regions of the conformer show (c) burial of K11 and potential salt bridge formation between K11 and E34, (d) burial of K29 and salt bridge formation between E16, D21, and K29, (e) salt bridge formation between K48 and D52 as well as between E51 and R54, and (f) salt bridge formation between K63 and E64. Dashed circles indicate salt bridge formations. The distances between carboxylic oxygen and amine hydrogen atoms are less than 4 Å.

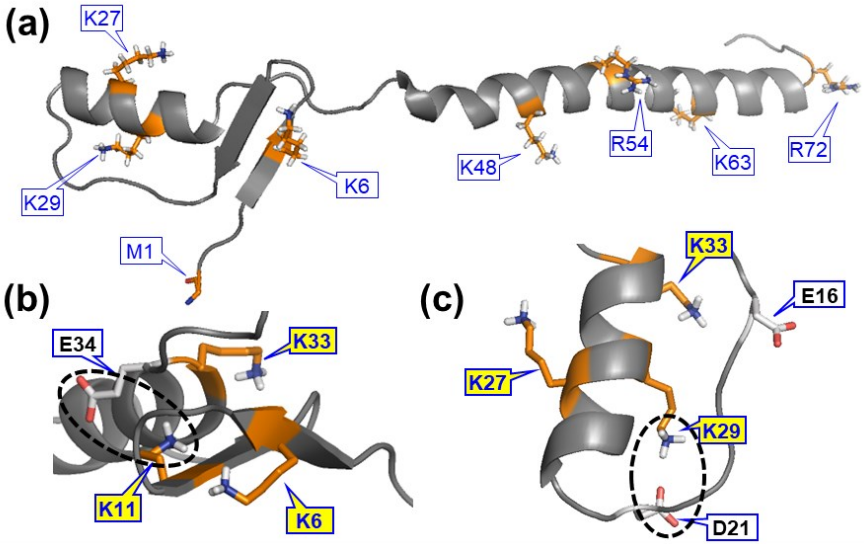

Figure 6. (a) A selected conformer from Figure 5a at CCS = 1772.86 Å^2 shows local regions highlighting (b) burial of K11 and (c) exposure of K29 due to disruption of the salt bridge with E16. Dashed circles indicate salt bridge formations. The distances between carboxylic oxygen and amine hydrogen atoms are less than 4 Å.

CONCLUSIONS

We have leveraged enhanced reagent reactivity and more extensive protein fragmentation to expand the exploration of gas-phase protein crosslinking. Compared to prior methods that use a singly deprotonated sulfo-EGS cross-linker (*i.e.* without a sodium ion present in the reagent), using a $[\text{sulfo-EGS} - 2\text{H} + \text{Na}]^-$ reagent provides enhanced reactivity at additional protonated amino acid residues that is not accessible with $[\text{sulfo-EGS} - \text{H}]^-$. Future work investigating the effect of sodium transfer on gas-phase sulfo-NHS chemistry will enable more detailed mechanistic insight. Additionally, the use of IRMPD here to effect more extensive consecutive protein fragmentation allowed for the facile generation of covalently modified internal fragment ions, which aided in covalent linkage site identification. These results indicate that 8+ A-state ubiquitin in the gas phase mostly preserves the solution-phase structure, exhibiting two gas-phase conformers with compact conformations in the N-terminal half of the protein. This subtle change in the local secondary and tertiary structures in the gas phase protein could not be detected without the improved sensitivity of this method. Overall, this gas-phase XL-MS method represents a useful tool to complement conventional high-resolution approaches in structural biology, providing for rapid structural evaluation with high sensitivity to differentiate gas-phase conformers.

ACKNOWLEDGEMENTS

This work was supported by the National Institutes of Health (NIH) under Awards R01GM138660 (BMP) and 1R01GM149646 (AP) (National Institute of General Medical Sciences (NIGMS)) and a contribution from Eli Lilly and Company. W-Y.K. and J.R.B.

acknowledge receipt of a University of Florida Graduate Student Funding Award (UF GSFA) Fellowship and J.R.B. acknowledges receipt of a UF CLAS Dissertation Fellowship.

REFERENCES

(1) James, L. C.; Tawfik, D. S. Conformational diversity and protein evolution – a 60-year-old hypothesis revisited. *Trends in Biochemical Sciences* **2003**, *28* (7), 361-368. DOI: https://doi.org/10.1016/S0968-0004(03)00135-X.

(2) Hartl, F. U. Protein Misfolding Diseases. *Annual Review of Biochemistry* **2017**, *86* (1), 21-26. DOI: 10.1146/annurev-biochem-061516-044518 (acccessed 2023/02/16).

(3) Banerjee, A.; Bhakta, S.; Sengupta, J. Integrative approaches in cryogenic electron microscopy: Recent advances in structural biology and future perspectives. *iScience* **2021**, *24* (2), 102044. DOI: https://doi.org/10.1016/j.isci.2021.102044.

(4) Chari, A.; Stark, H. Prospects and Limitations of High-Resolution Single-Particle Cryo-Electron Microscopy. *Annual Review of Biophysics* **2023**, *52* (1), 391-411. DOI: 10.1146/annurev-biophys-111622-091300 (acccessed 2024/01/17).

(5) Lucas, B. A. Visualizing everything, everywhere, all at once: Cryo-EM and the new field of structureomics. *Current Opinion in Structural Biology* **2023**, *81*, 102620. DOI: https://doi.org/10.1016/j.sbi.2023.102620.

(6) Harrison, P. J.; Vecerkova, T.; Clare, D. K.; Quigley, A. A review of the approaches used to solve sub-100 kDa membrane proteins by cryo-electron microscopy. *Journal of Structural Biology* **2023**, *215* (2), 107959. DOI: https://doi.org/10.1016/j.jsb.2023.107959.

(7) Wüthrich, K. Protein structure determination in solution by NMR spectroscopy. *Journal of Biological Chemistry* **1990**, *265* (36), 22059-22062. DOI: https://doi.org/10.1016/S0021-9258(18)45665-7.

(8) Ishima, R.; Torchia, D. A. Protein dynamics from NMR. *Nature Structural Biology* **2000**, *7* (9), 740-743. DOI: 10.1038/78963.

(9) Shi, Y. A Glimpse of Structural Biology through X-Ray Crystallography. *Cell* **2014**, *159* (5), 995-1014. DOI: https://doi.org/10.1016/j.cell.2014.10.051.

(10) Smyth, M. S.; Martin, J. H. J. x Ray crystallography. *Molecular Pathology* **2000**, *53* (1), 8. DOI: 10.1136/mp.53.1.8.

(11) Kaltashov, I. A.; Eyles, S. J. Studies of biomolecular conformations and conformational dynamics by mass spectrometry. *Mass Spectrometry Reviews* **2002**, *21* (1), 37-71. DOI: 10.1002/mas.10017 Readcube.

(12) Petrotchenko, E. V.; Borchers, C. H. Protein Chemistry Combined with Mass Spectrometry for Protein Structure Determination. *Chemical Reviews* **2022**, *122* (8), 7488-7499. DOI: 10.1021/acs.chemrev.1c00302.

(13) Straus, R. N.; Jockusch, R. A. Hydrogen-Deuterium Exchange and Electron Capture Dissociation to Interrogate the Conformation of Gaseous Melittin Ions. *Journal of the American Society for Mass Spectrometry* **2019**, *30* (5), 864-875. DOI: 10.1007/s13361-019-02150-5.

(14) Sanguantrakun, N.; Chanthamontri, C.; Gross, M. L. Top-Down Analysis of In-Source HDX of Native Protein Ions. *Journal of the American Society for Mass Spectrometry* **2020**, *31* (5), 1151-1154. DOI: 10.1021/jasms.9b00149.

(15) Chaturvedi, R.; Webb, I. K. Multiplexed Conformationally Selective, Localized Gas-Phase Hydrogen Deuterium Exchange of Protein Ions Enabled by Transmission-Mode Electron Capture Dissociation. *Analytical Chemistry* **2022**, *94* (25), 8975-8982. DOI: 10.1021/acs.analchem.2c00942.

(16) Zhang, H.; Cui, W.; Gross, M. L. Native electrospray ionization and electron-capture dissociation for comparison of protein structure in solution and the gas phase. *International Journal of Mass Spectrometry* **2013**, *354-355*, 288-291. DOI: https://doi.org/10.1016/j.ijms.2013.06.019.
(17) Lam, Y. P. Y.; Wootton, C. A.; Hands-Portman, I.; Wei, J.; Chiu, C. K. C.; Romero-Canelon, I.; Lermyte, F.; Barrow, M. P.; O'Connor, P. B. Determination of the Aggregate Binding Site of Amyloid Protofibrils Using Electron Capture Dissociation Tandem Mass Spectrometry. *Journal of the American Society for Mass Spectrometry* **2020**, *31* (2), 267-276. DOI: 10.1021/jasms.9b00053.
(18) Williams, J. P.; Morrison, L. J.; Brown, J. M.; Beckman, J. S.; Voinov, V. G.; Lermyte, F. Top-Down Characterization of Denatured Proteins and Native Protein Complexes Using Electron Capture Dissociation Implemented within a Modified Ion Mobility-Mass Spectrometer. *Analytical Chemistry* **2020**, *92* (5), 3674-3681. DOI: 10.1021/acs.analchem.9b04763.
(19) Breuker, K.; Oh, H.; Horn, D. M.; Cerda, B. A.; McLafferty, F. W. Detailed Unfolding and Folding of Gaseous Ubiquitin Ions Characterized by Electron Capture Dissociation. *Journal of the American Chemical Society* **2002**, *124* (22), 6407-6420. DOI: 10.1021/ja012267j.
(20) Theisen, A.; Black, R.; Corinti, D.; Brown, J. M.; Bellina, B.; Barran, P. E. Initial Protein Unfolding Events in Ubiquitin, Cytochrome c and Myoglobin Are Revealed with the Use of 213 nm UVPD Coupled to IM-MS. *Journal of the American Society for Mass Spectrometry* **2019**, *30* (1), 24-33. DOI: 10.1007/s13361-018-1992-0.
(21) Blevins, M. S.; Walker, J. N.; Schaub, J. M.; Finkelstein, I. J.; Brodbelt, J. S. Characterization of the T4 gp32–ssDNA complex by native, cross-linking, and ultraviolet photodissociation mass spectrometry. *Chemical Science* **2021**, *12* (41), 13764-13776, 10.1039/D1SC02861H. DOI: 10.1039/D1SC02861H.
(22) Santos, I. C.; Brodbelt, J. S. Structural Characterization of Carbonic Anhydrase–Arylsulfonamide Complexes Using Ultraviolet Photodissociation Mass Spectrometry. *Journal of the American Society for Mass Spectrometry* **2021**, *32* (6), 1370-1379. DOI: 10.1021/jasms.1c00004.
(23) Kruppa, G. H.; Schoeniger, J.; Young, M. M. A top down approach to protein structural studies using chemical cross-linking and Fourier transform mass spectrometry. *Rapid Communications in Mass Spectrometry* **2003**, *17* (2), 155-162, https://doi.org/10.1002/rcm.885. DOI: https://doi.org/10.1002/rcm.885 (acccessed 2022/12/13).
(24) Chakravarti, B.; Lewis, J. S.; Chakravarti, N. D.; Raval, A. Three Dimensional Structures of Proteins and Protein Complexes from Chemical Cross-Linking and Mass Spectrometry: A Biochemical and Computational Overview. *Current Proteomics* **2006**, *3* (1), 1-21. DOI: http://dx.doi.org/10.2174/157016406777145694.
(25) Sinz, A. Chemical cross-linking and mass spectrometry to map three-dimensional protein structures and protein–protein interactions. *Mass Spectrometry Reviews* **2006**, *25* (4), 663-682, https://doi.org/10.1002/mas.20082. DOI: https://doi.org/10.1002/mas.20082 (acccessed 2022/12/13).
(26) Piersimoni, L.; Kastritis, P. L.; Arlt, C.; Sinz, A. Cross-Linking Mass Spectrometry for Investigating Protein Conformations and Protein–Protein Interactions─A Method for All

Seasons. *Chemical Reviews* **2022**, *122* (8), 7500-7531. DOI: 10.1021/acs.chemrev.1c00786.
(27) Singh, P.; Panchaud, A.; Goodlett, D. R. Chemical cross-linking and mass spectrometry as a low-resolution protein structure determination technique. *Analytical Chemistry* **2010**, *82* (7), 2636-2642. DOI: 10.1021/ac1000724 Readcube.
(28) Piersimoni, L.; Sinz, A. Cross-linking/mass spectrometry at the crossroads. *Analytical and Bioanalytical Chemistry* **2020**, *412* (24), 5981-5987. DOI: 10.1007/s00216-020-02700-x.
(29) Webb, I. K.; Mentinova, M.; McGee, W. M.; McLuckey, S. A. Gas-Phase Intramolecular Protein Crosslinking via Ion/Ion Reactions: Ubiquitin and a Homobifunctional sulfo-NHS Ester. *Journal of The American Society for Mass Spectrometry* **2013**, *24* (5), 733-743. DOI: 10.1007/s13361-013-0590-4.
(30) Cheung See Kit, M.; Carvalho, V. V.; Vilseck, J. Z.; Webb, I. K. Gas-phase ion/ion chemistry for structurally sensitive probes of gaseous protein ion structure: Electrostatic and electrostatic to covalent cross-linking. *International Journal of Mass Spectrometry* **2021**, *463*, 116549. DOI: https://doi.org/10.1016/j.ijms.2021.116549.
(31) Cheung See Kit, M.; Webb, I. K. Application of Multiple Length Cross-linkers to the Characterization of Gaseous Protein Structure. *Analytical Chemistry* **2022**. DOI: 10.1021/acs.analchem.2c03044.
(32) Bu, J.; Fisher, C. M.; Gilbert, J. D.; Prentice, B. M.; McLuckey, S. A. Selective Covalent Chemistry via Gas-Phase Ion/ion Reactions: An Exploration of the Energy Surfaces Associated with N-Hydroxysuccinimide Ester Reagents and Primary Amines and Guanidine Groups. *Journal of the American Society for Mass Spectrometry* **2016**, *27* (6), 1089-1098. DOI: 10.1007/s13361-016-1359-3.
(33) Xia, Y.; McLuckey, S. A. Evolution of instrumentation for the study of gas-phase ion/ion chemistry via mass spectrometry. *Journal of the American Society for Mass Spectrometry* **2008**, *19* (2), 173-189. DOI: 10.1016/j.jasms.2007.10.018 PubMed.
(34) Prentice, B. M.; McLuckey, S. A. Gas-phase ion/ion reactions of peptides and proteins: acid/base, redox, and covalent chemistries. *Chemical Communications* **2013**, *49* (10), 947-965. DOI: 10.1039/c2cc36577d Readcube.
(35) Foreman, D. J.; McLuckey, S. A. Recent Developments in Gas-Phase Ion/Ion Reactions for Analytical Mass Spectrometry. *Analytical Chemistry* **2020**, *92* (1), 252-266. DOI: 10.1021/acs.analchem.9b05014.
(36) Pitteri, S. J.; McLuckey, S. A. Recent developments in the ion/ion chemistry of high-mass multiply charged ions. *Mass Spectrometry Reviews* **2005**, *24* (6), 931-958. DOI: 10.1002/mas.20048 Readcube.
(37) McLuckey, S. A.; Huang, T.-Y. Ion/Ion Reactions: New Chemistry for Analytical MS. *Analytical Chemistry* **2009**, *81* (21), 8669-8676. DOI: 10.1021/ac9014935.
(38) Cammarata, M. B.; Brodbelt, J. S. Characterization of Intra- and Intermolecular Protein Crosslinking by Top Down Ultraviolet Photodissociation Mass Spectrometry. *ChemistrySelect* **2016**, *1* (3), 590-593, https://doi.org/10.1002/slct.201600140. DOI: https://doi.org/10.1002/slct.201600140 (acccessed 2022/12/13).
(39) Ding, Y.-H.; Fan, S.-B.; Li, S.; Feng, B.-Y.; Gao, N.; Ye, K.; He, S.-M.; Dong, M.-Q. Increasing the Depth of Mass-Spectrometry-Based Structural Analysis of Protein Complexes through the Use of Multiple Cross-Linkers. *Analytical Chemistry* **2016**, *88* (8), 4461-4469. DOI: 10.1021/acs.analchem.6b00281.

(40) Brodie, N. I.; Popov, K. I.; Petrotchenko, E. V.; Dokholyan, N. V.; Borchers, C. H. Conformational ensemble of native α-synuclein in solution as determined by short-distance crosslinking constraint-guided discrete molecular dynamics simulations. *PLOS Computational Biology* **2019**, *15* (3), e1006859. DOI: 10.1371/journal.pcbi.1006859.
(41) Prentice, B. M.; McGee, W. M.; Stutzman, J. R.; McLuckey, S. A. Strategies for the gas phase modification of cationized arginine via ion/ion reactions. *International Journal of Mass Spectrometry* **2013**, *354-355*, 211-218. DOI: https://doi.org/10.1016/j.ijms.2013.05.026.
(42) Cobb, J. S.; Easterling, M. L.; Agar, J. N. Structural characterization of intact proteins is enhanced by prevalent fragmentation pathways rarely observed for peptides. *Journal of the American Society for Mass Spectrometry* **2010**, *21* (6), 949-959. DOI: 10.1016/j.jasms.2010.02.009.
(43) Durbin, K. R.; Skinner, O. S.; Fellers, R. T.; Kelleher, N. L. Analyzing Internal Fragmentation of Electrosprayed Ubiquitin Ions During Beam-Type Collisional Dissociation. *Journal of the American Society for Mass Spectrometry* **2015**, *26* (5), 782-787. DOI: 10.1007/s13361-015-1078-1.
(44) Wei, B.; Zenaidee, M. A.; Lantz, C.; Ogorzalek Loo, R. R.; Loo, J. A. Towards understanding the formation of internal fragments generated by collisionally activated dissociation for top-down mass spectrometry. *Analytica Chimica Acta* **2022**, *1194*, 339400. DOI: https://doi.org/10.1016/j.aca.2021.339400.
(45) Wei, B.; Zenaidee, M. A.; Lantz, C.; Williams, B. J.; Totten, S.; Ogorzalek Loo, R. R.; Loo, J. A. Top-down mass spectrometry and assigning internal fragments for determining disulfide bond positions in proteins. *Analyst* **2023**, 10.1039/D2AN01517J. DOI: 10.1039/D2AN01517J.
(46) Schmitt, N. D.; Berger, J. M.; Conway, J. B.; Agar, J. N. Increasing Top-Down Mass Spectrometry Sequence Coverage by an Order of Magnitude through Optimized Internal Fragment Generation and Assignment. *Analytical Chemistry* **2021**, *93* (16), 6355-6362. DOI: 10.1021/acs.analchem.0c04670.
(47) Zhou, R. Replica Exchange Molecular Dynamics Method for Protein Folding Simulation. In *Protein Folding Protocols*, Bai, Y., Nussinov, R. Eds.; Humana Press, 2006; pp 205-223.
(48) Sztáray, J.; Memboeuf, A.; Drahos, L.; Vékey, K. Leucine enkephalin—A mass spectrometry standard. *Mass Spectrometry Reviews* **2011**, *30* (2), 298-320. DOI: https://doi.org/10.1002/mas.20279 (acccessed 2023/10/09).
(49) Bonney, J. R.; Kang, W.-Y.; Specker, J. T.; Liang, Z.; Scoggins, T. R. I. V.; Prentice, B. M. Relative Quantification of Lipid Isomers in Imaging Mass Spectrometry Using Gas-Phase Charge Inversion Ion/Ion Reactions and Infrared Multiphoton Dissociation. *Analytical Chemistry* **2023**, *95* (48), 17766-17775. DOI: 10.1021/acs.analchem.3c03804.
(50) Baker, P. R., Clauser, K.R. *Protein Prospector*. http://prospector.ucsf.edu (accessed.
(51) Kaplan, D. A.; Hartmer, R.; Speir, J. P.; Stoermer, C.; Gumerov, D.; Easterling, M. L.; Brekenfeld, A.; Kim, T.; Laukien, F.; Park, M. A. Electron transfer dissociation in the hexapole collision cell of a hybrid quadrupole-hexapole Fourier transform ion cyclotron resonance mass spectrometer. *Rapid Communications in Mass Spectrometry* **2008**, *22* (3), 271-278, https://doi.org/10.1002/rcm.3356. DOI: https://doi.org/10.1002/rcm.3356 (acccessed 2021/05/06).

(52) Specker, J. T.; Van Orden, S. L.; Ridgeway, M. E.; Prentice, B. M. Identification of Phosphatidylcholine Isomers in Imaging Mass Spectrometry Using Gas-Phase Charge Inversion Ion/Ion Reactions. *Analytical Chemistry* **2020**, *92* (19), 13192-13201. DOI: 10.1021/acs.analchem.0c02350.
(53) Specker, J. T.; Prentice, B. M. Separation of Isobaric Lipids in Imaging Mass Spectrometry Using Gas-Phase Charge Inversion Ion/Ion Reactions. *Journal of the American Society for Mass Spectrometry* **2023**, *34* (9), 1868-1878. DOI: 10.1021/jasms.3c00081.
(54) Diao, X.; Ellin, N. R.; Prentice, B. M. Selective Schiff base formation via gas-phase ion/ion reactions to enable differentiation of isobaric lipids in imaging mass spectrometry. *Analytical and Bioanalytical Chemistry* **2023**, *415* (18), 4319-4331. DOI: 10.1007/s00216-023-04523-y.
(55) Bonney, J. R.; Prentice, B. M. Structural Elucidation and Relative Quantification of Fatty Acid Double Bond Positional Isomers in Biological Tissues Enabled by Gas-Phase Charge Inversion Ion/Ion Reactions. *Analysis & Sensing* **2023**, *n/a* (n/a), e202300063. DOI: https://doi.org/10.1002/anse.202300063 (acccessed 2024/01/17).
(56) Brutscher, B.; Brüschweiler, R.; Ernst, R. R. Backbone Dynamics and Structural Characterization of the Partially Folded A State of Ubiquitin by 1H, 13C, and 15N Nuclear Magnetic Resonance Spectroscopy. *Biochemistry* **1997**, *36* (42), 13043-13053. DOI: 10.1021/bi971538t.
(57) Stockman, B. J.; Euvrard, A.; Scahill, T. A. Heteronuclear three-dimensional NMR spectroscopy of a partially denatured protein: The A-state of human ubiquitin. *Journal of Biomolecular NMR* **1993**, *3* (3), 285-296. DOI: 10.1007/BF00212515.
(58) Cordier, F.; Grzesiek, S. Quantitative Comparison of the Hydrogen Bond Network of A-State and Native Ubiquitin by Hydrogen Bond Scalar Couplings. *Biochemistry* **2004**, *43* (35), 11295-11301. DOI: 10.1021/bi049314f.
(59) Onufriev, A. Chapter 7 - Implicit Solvent Models in Molecular Dynamics Simulations: A Brief Overview. In *Annual Reports in Computational Chemistry*, Wheeler, R. A., Spellmeyer, D. C. Eds.; Vol. 4; Elsevier, 2008; pp 125-137.
(60) Nguyen, H.; Roe, D. R.; Simmerling, C. Improved Generalized Born Solvent Model Parameters for Protein Simulations. *Journal of Chemical Theory and Computation* **2013**, *9* (4), 2020-2034. DOI: 10.1021/ct3010485.
(61) Maier, J. A.; Martinez, C.; Kasavajhala, K.; Wickstrom, L.; Hauser, K. E.; Simmerling, C. ff14SB: Improving the Accuracy of Protein Side Chain and Backbone Parameters from ff99SB. *Journal of Chemical Theory and Computation* **2015**, *11* (8), 3696-3713. DOI: 10.1021/acs.jctc.5b00255.
(62) Hornak, V.; Abel, R.; Okur, A.; Strockbine, B.; Roitberg, A.; Simmerling, C. Comparison of multiple Amber force fields and development of improved protein backbone parameters. *Proteins: Structure, Function, and Bioinformatics* **2006**, *65* (3), 712-725, https://doi.org/10.1002/prot.21123. DOI: https://doi.org/10.1002/prot.21123 (acccessed 2023/01/10).
(63) Wickstrom, L.; Okur, A.; Simmerling, C. Evaluating the Performance of the ff99SB Force Field Based on NMR Scalar Coupling Data. *Biophysical Journal* **2009**, *97* (3), 853-856. DOI: https://doi.org/10.1016/j.bpj.2009.04.063.
(64) Perez, A.; MacCallum, J. L.; Dill, K. A. Accelerating molecular simulations of proteins using Bayesian inference on weak information. *Proceedings of the National Academy of*

Sciences **2015**, *112* (38), 11846-11851. DOI: 10.1073/pnas.1515561112 (acccessed 2022/12/14).
(65) MacCallum, J. L.; Perez, A.; Dill, K. A. Determining protein structures by combining semireliable data with atomistic physical models by Bayesian inference. *Proceedings of the National Academy of Sciences* **2015**, *112* (22), 6985-6990. DOI: 10.1073/pnas.1506788112 (acccessed 2022/12/14).
(66) Roe, D. R.; Cheatham, T. E., III. PTRAJ and CPPTRAJ: Software for Processing and Analysis of Molecular Dynamics Trajectory Data. *Journal of Chemical Theory and Computation* **2013**, *9* (7), 3084-3095. DOI: 10.1021/ct400341p.
(67) Arcella, A.; Portella, G.; Ruiz, M. L.; Eritja, R.; Vilaseca, M.; Gabelica, V.; Orozco, M. Structure of Triplex DNA in the Gas Phase. *Journal of the American Chemical Society* **2012**, *134* (15), 6596-6606. DOI: 10.1021/ja209786t.
(68) Case, D. A.; Cheatham Iii, T. E.; Darden, T.; Gohlke, H.; Luo, R.; Merz Jr, K. M.; Onufriev, A.; Simmerling, C.; Wang, B.; Woods, R. J. The Amber biomolecular simulation programs. *Journal of Computational Chemistry* **2005**, *26* (16), 1668-1688, https://doi.org/10.1002/jcc.20290. DOI: https://doi.org/10.1002/jcc.20290 (acccessed 2023/01/10).
(69) Ewing, S. A.; Donor, M. T.; Wilson, J. W.; Prell, J. S. Collidoscope: An Improved Tool for Computing Collisional Cross-Sections with the Trajectory Method. *Journal of the American Society for Mass Spectrometry* **2017**, *28* (4), 587-596. DOI: 10.1007/s13361-017-1594-2.
(70) Myung, S.; Badman, E. R.; Lee, Y. J.; Clemmer, D. E. Structural Transitions of Electrosprayed Ubiquitin Ions Stored in an Ion Trap over ~10 ms to 30 s. *The Journal of Physical Chemistry A* **2002**, *106* (42), 9976-9982. DOI: 10.1021/jp0206368.
(71) Little, D. P.; Speir, J. P.; Senko, M. W.; O'Connor, P. B.; McLafferty, F. W. Infrared Multiphoton Dissociation of Large Multiply Charged Ions for Biomolecule Sequencing. *Analytical Chemistry* **1994**, *66* (18), 2809-2815. DOI: 10.1021/ac00090a004.
(72) Novak, P.; Young, M. M.; Schoeniger, J. S.; Kruppa, G. H. A Top-Down Approach to Protein Structure Studies Using Chemical Cross-Linking and Fourier Transform Mass Spectrometry. *European Journal of Mass Spectrometry* **2003**, *9* (6), 623-631. DOI: 10.1255/ejms.590 (acccessed 2024/01/03).
(73) Bleiholder, C.; Liu, F. C. Structure Relaxation Approximation (SRA) for Elucidation of Protein Structures from Ion Mobility Measurements. *The Journal of Physical Chemistry B* **2019**, *123* (13), 2756-2769. DOI: 10.1021/acs.jpcb.8b11818.
(74) Meyer, T.; Gabelica, V.; Grubmüller, H.; Orozco, M. Proteins in the gas phase. *WIREs Computational Molecular Science* **2013**, *3* (4), 408-425, https://doi.org/10.1002/wcms.1130. DOI: https://doi.org/10.1002/wcms.1130 (acccessed 2022/12/14).
(75) Morrison, L. J.; Brodbelt, J. S. Charge site assignment in native proteins by ultraviolet photodissociation (UVPD) mass spectrometry. *Analyst* **2016**, *141* (1), 166-176, 10.1039/C5AN01819F. DOI: 10.1039/C5AN01819F.